Pergamon

Engineering Fracture Mechanics Vol. 48, No. 5, pp. 673–689, 1994

0013-7944/94 $7.00 + 0.00

SCALING LAWS FOR STRENGTH AND TOUGHNESS OF DISORDERED MATERIALS: A UNIFIED THEORY BASED ON FRACTAL GEOMETRY

ALBERTO CARPINTERI
Politecnico di Torino, Department of Structural Engineering, 10129 Torino, Italy
GERARDO FERRARA
ENEL, Research Centre for Hydraulics and Structural Engineering, 20162 Milano, Italy
and
LORENZO IMPERATO
ISMES, 24100 Bergamo, Italy

Abstract—Direct tensile testing of concrete was carried out in a stable manner and the deformation eccentricity was adjusted continuously during the loading process. In this way, the secondary flexural stresses were minimized so that it was possible to obtain nominal tensile strength and fracture energy of the material. Both such properties appear to vary monotonically with the diameter of the cylindrical specimens: the tensile strength decreases, whereas the fracture energy increases. For disordered materials it is impossible to measure constant material properties, unless we depart from integer dimensions of the material ligament at peak stress and of the fracture surface at final rupture, in the framework of fractal geometry. In this way we can define new tensile properties with physical dimensions depending on the fractal dimension of the damaged microstructure, which turn out to be scale-invariant material constants. This represents the so-called renormalization procedure, already proposed in the statistical physics of random processes. As a limit case, when the material is extremely disordered, both tensile strength and fracture energy present the physical dimension characteristic of the stress-intensity factor, $[F]\,[L]^{-3/2}$.

1. INTRODUCTION

DIRECT TENSILE testing of concrete is difficult to perform in practice, and even though some investigators have already proposed different testing methods, the problem has not yet been solved. These methods have been, for the most part, influenced by secondary flexural stresses and do not produce a purely tensile load [1–10].

On behalf of ENEL-DRS-CRIS, Milan, an experimental research programme has been carried out at the Static Tests Division of ISMES in Bergamo on fracture mechanics applied to concrete with the following aims in view:

(a) to set up a test apparatus for performing stable tensile tests, able to operate on specimens of large dimensions (maximum diameter 30 cm).
(b) to conduct an articulated programme of tensile tests for verifying the variability of the tensile parameters σ_u and $\mathcal{G}_F$—tensile strength and fracture energy—with the variation of specimen size.

The material making up the test specimens was to be of the same type used in ref. [11]. The concrete mixture was made with gravel (maximum diameter, 25 mm), 2.80 kN/m^3 of Portland 325 cement and a water/cement ratio equal to 0.43.

This paper describes the loading and measuring equipment used, sets forth the procedure according to which the tests were performed and presents diagrams of the values of the measurements performed. Tensile strength and fracture energy prove to vary monotonically with the diameter of the cylindrical specimens.

In the second part of the paper the problems of the size effects on tensile strength and fracture energy are reconsidered under a new and unifying light cast by fractal geometry [12, 13]. It is physically impossible to measure constant material properties, unless we depart from integer dimensions of the material ligament at peak stress and of the fracture surface at final rupture. In this way we can define new tensile properties with physical dimensions depending on the fractal

dimension of the damaged microstructure, which turn out to be scale-invariant material constants. This represents the so-called renormalization procedure, already proposed in the statistical physics of random processes [14, 15]. Variations in the fractal dimension of fracture surfaces produce variations in the physical dimension of toughness, and not, as asserted by some authors, only in the measure of toughness [16]. In disordered materials, an attenuation of the size effects due to the dimensional disparity between strength and toughness is found. As a limit case, any size effect vanishes when both tensile strength and fracture energy present the physical dimension characteristic of the stress-intensity factor, $[F]\,[L]^{-3/2}$. It is very likely that this critical situation is achieved only inside a very disordered damaged microstructure, e.g. in the vicinity of the crack tip. In the case of tensile strength, the dimensional decrement represents self-similar weakening of the material ligament, due to pores, voids, defects, cracks, aggregates, inclusions, etc. Analogously, in the case of fracture energy, the dimensional increment represents self-similar tortuosity of the fracture surface, as well as self-similar overlapping and distribution of microcracks in a direction orthogonal to that of the forming macrocrack.

2. STABLE TENSILE TESTS

Fracture energy $\mathscr{G}_F$ currently represents the most significant parameter for describing the mechanical features of a quasi-brittle material (concrete, rocks, ceramics, etc.) subjected to stress-concentration phenomena, such as those involved in the propagation of a crack.

The parameter $\mathscr{G}_F$ is defined as "the amount of energy needed to create a crack of unit surface". If we consider a one-dimensional sample subjected to a direct tensile load, by adopting particular testing techniques it is possible to determine the complete stress–strain curve. Initially the material behaves elastically, then, as the load increases, it begins to obey a nonlinear law on account of the appearance of microcracks distributed throughout the test specimen. When the maximum tensile strength of the material is reached, the weakest cross-section of the sample is no longer able to withstand further load increments, and hence there is a concentration of microcracks developing which is limited to that cross-section. This means that once the maximum load is reached, the phenomenon of microcracking allows further increments of strain to occur in the volume of cracked material (fracture zone), whilst the material outside that volume undergoes elastic unloading. The increase in the global deformation of the specimen proceeds until the process of microcrack propagation has developed and extended right through the entire cross-section, with a gradual reduction and eventually annulling of the load.

The energy balance at the end of the test is represented by the equality between the work performed from outside and the energy initially dissipated owing to inelastic effects and then consumed for crack propagation. This energy is represented geometrically by the area under the stress-crack opening curve. The experimental value of this cracking energy, divided by the projection of the fracture surface, yields the specific fracture energy, denoted by the symbol $\mathscr{G}_F$.

3. TEST EQUIPMENT SETUP

3.1. *Stable tensile tests using servo-controlled hydraulic systems*

The setup of the experimental technique was first performed on pre-notched prismatic specimens having a minimum cross-section of 100 × 100 mm. The first tests immediately provided an indication of the influence of certain factors with regard to the stability of the test, such as:

Sample preparation, i.e. respect of perfect parallelism of the surfaces to be glued, their orthogonality to the vertical axis, as well as their precise flatness. This requirement derived also from the fact that the loading apparatus, not being equipped with ball joints, had to impose the increment of the strain in the specimen, mechanically maintaining its end surfaces perfectly parallel. The failure to adopt the latter essential expedient inevitably produced tenso-flexures which led to failure of the specimen outside the pre-notched section, usually in fairly close vicinity to the area where the specimen was glued to the plates.

Limited length of the sample, which in no case was greater than twice the dimension of the side.

The loading equipment used to conduct the stable direct tensile tests on concrete specimens is illustrated in Fig. 1(b) as well as in the photograph of Fig. 1(a). It consists of a cylindrical tubular

element inside which the specimen is placed, the two upper and lower bases being glued, respectively, to the upper lid of the cylinder and to a metal plate with a threaded stem, previously screwed into the hole of the hydraulic actuator piston.

The cylinder and the external structure of the actuator constitute a counter-reaction to the tensile force exerted by the piston, which is controlled so as to impose an increasing strain at the site of the notch at a slow rate and in obedience to a linear law.

3.2. *Test procedure*

The test was carried out according to an experimental procedure which involved the following phases.

(A) *Placing of test specimen in the apparatus.* Position the piston up against the upper stop of the actuator (Fig. 2). Screw the threaded stem of the lower plate in the piston hole and tighten (Fig. 3). Glue the specimen on the plate, which is held rigidly to the actuator piston, using fast-hardening cyanoacrylate resin adhesive (Fig. 4). Mount the three instruments for checking

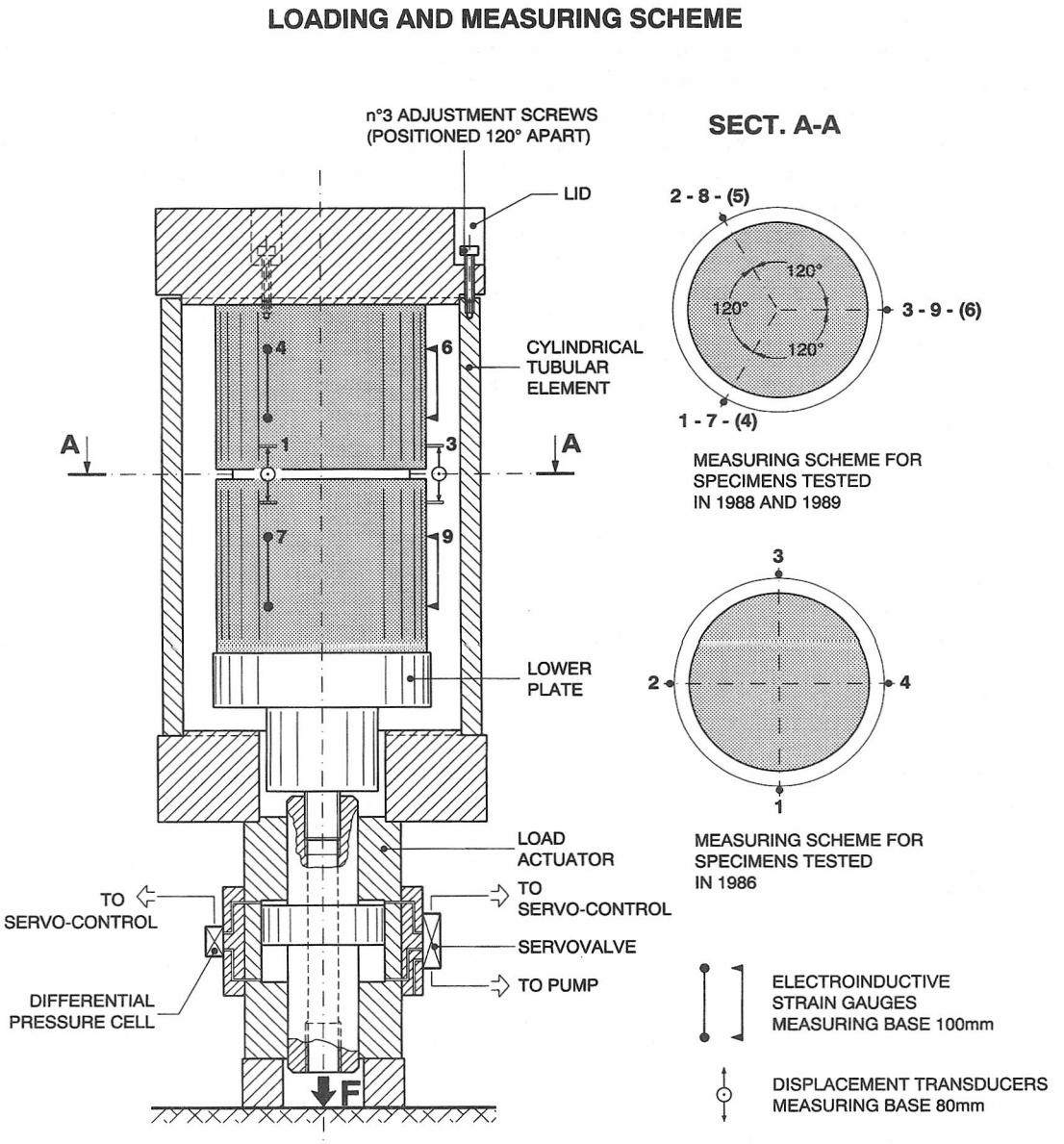

Fig 1(b). Loading and measuring scheme.

and controlling crack opening displacement on the three bases previously drawn at 120° from one another (Fig. 5). For certain specimens with suitable geometry, measurement was made of the strains in the upper and lower portions of the specimen (Fig. 6). Position the steel lid, equipped with adjustment screws, set in their seats on the upper rim of the steel reaction tube. Line up the steel lid against the upper end plane of the specimen, via suitable adjustment of the three screws. Adjust the screws until their lower tips make contact with their seats. Once contact was made, care was taken not to screw them down too vigorously or too tightly. Raise the lid, apply the adhesive on the upper face of the test specimen (Fig. 7), and, finally, lower the lid so that the adjustment screws are properly positioned in their seats (Fig. 8). Wait for the adhesive to harden (approximately 30 min). Carry out a final check to ensure that the spherical tips of the adjustment screws make contact with their seats.

(B) *Phase of adjustment of deformation eccentricity under load.* This consisted of preparation of a diagram with a scale capable of amplifying the initial portion of the stress–strain curve; setting of control rate at $1\,\text{mm} \times 10^{-3}/100\,\text{sec}$; subjecting the test specimen to tension until a load was achieved that corresponds to a nominal stress in the notched section equal to 0.5 MPa, and subsequent interruption of the ramp; checking of the values of the three instruments and identification of the one that presented the smallest elongation; adjustment of the screw corresponding to the instrument that presented the smallest elongation, tightening it in such a way that the magnitudes of the strains recorded on the three instruments tended to be equal. This operation can be performed by acting on more than one adjustment screw; return to the zero of the load and check to see also that the strains return to zero, remaining equal to one another. In the event of this not occurring, the necessary correction was made by adjusting the screws, and the loading operation was repeated at 0.5 MPa.

(C) *Testing phase.* This consisted of startup of a tensile test conducted by applying a controlled strain, i.e. imposing a displacement equal to the average of the readings of the three instruments, and measuring the force applied. The change of the deformation rate when the crack opening displacement was equal to $50\,\text{mm} \times 10^{-3}$, bringing it to $1\,\text{mm} \times 10^{-3}/60\,\text{sec}$, as well as at $100\,\text{mm} \times 10^{-3}$ of the crack opening displacement, bringing it to $1\,\text{mm} \times 10^{-3}/20\,\text{sec}$; termination of the test when the load went to zero or when the crack opening displacement reached $300\,\text{mm} \times 10^{-3}$ (Fig. 9).

3.3. *Measuring instruments and data acquisition*

The position and numbering of the instruments used in the test are displayed in Fig. 1(b). The quantities recorded are represented by:

(1) The opening of the notch, detected by three Hottinger W1TK electro-inductive displacement transducers with 80 mm measurement bases.
(2) The global longitudinal strain of the specimen measured in six different positions by six Hottinger D1 electro-inductive extensometers (this was performed occasionally only on specimens of suitable geometry).
(3) Tensile force of the actuator measured by a differential pressure cell.

During the course of the tests, an automatic system of data acquisition recorded the signals coming from the measuring instruments, simultaneously storing them on magnetic medium for subsequent graphic data processing. The automatic system allowed the control of the test in real time via the numerical restitution of the instrument measurements and the plotting of the force–displacement curves on the screen.

4. EXPERIMENTAL RESULTS AND FRACTAL CONCEPTS

In the course of the experimental programme which extended over about three years, numerous tests were aimed principally at devising and setting up the loading and measuring equipment and the devices for deformation eccentricity adjustment, and at the choice of the best adhesive to use.

The tests were carried out on four specimen diameters: 12, 18, 24 and 30 cm. Different tests were performed for each diameter (Table 1). It is to be noted that the aspect ratio of the cylindrical

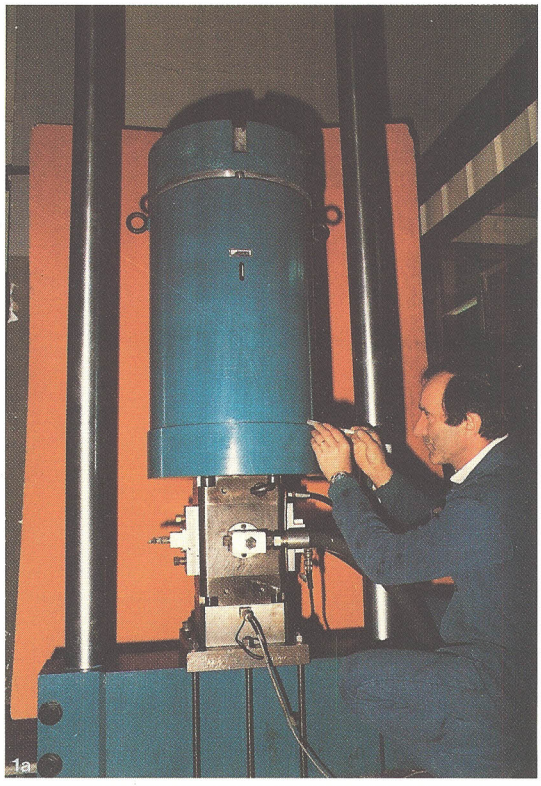

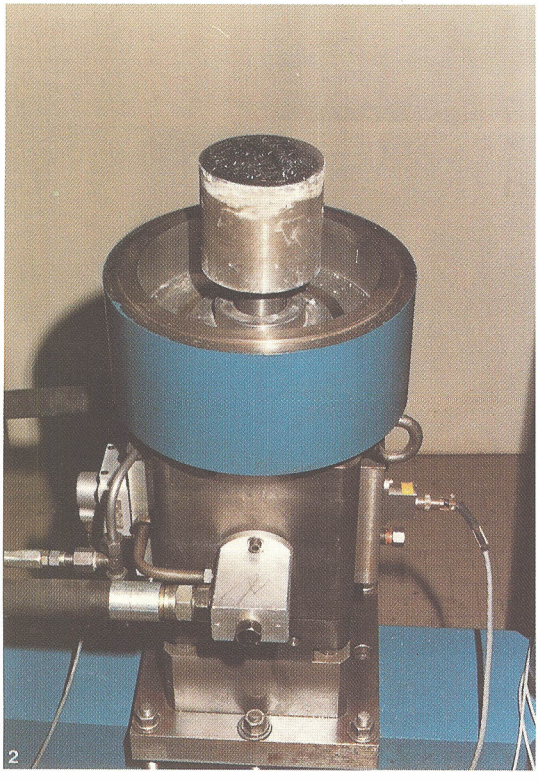

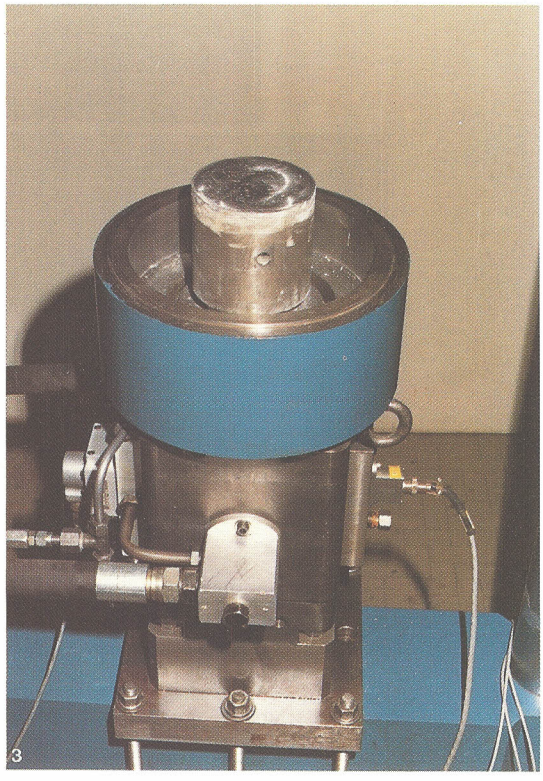

Fig. 1. (a) Loading equipment.
Fig. 2. Piston against upper stop of actuator.
Fig. 3. Screwing of threaded stem of lower plate in hole of actuator piston.

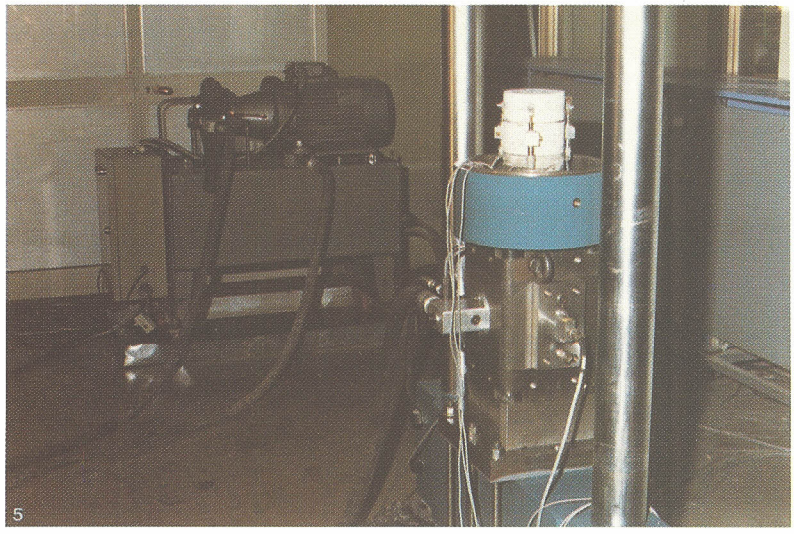

Fig. 4. Gluing of specimen on lower plate.
Fig. 5. Assembly of the three instruments for controlling crack opening displacement.

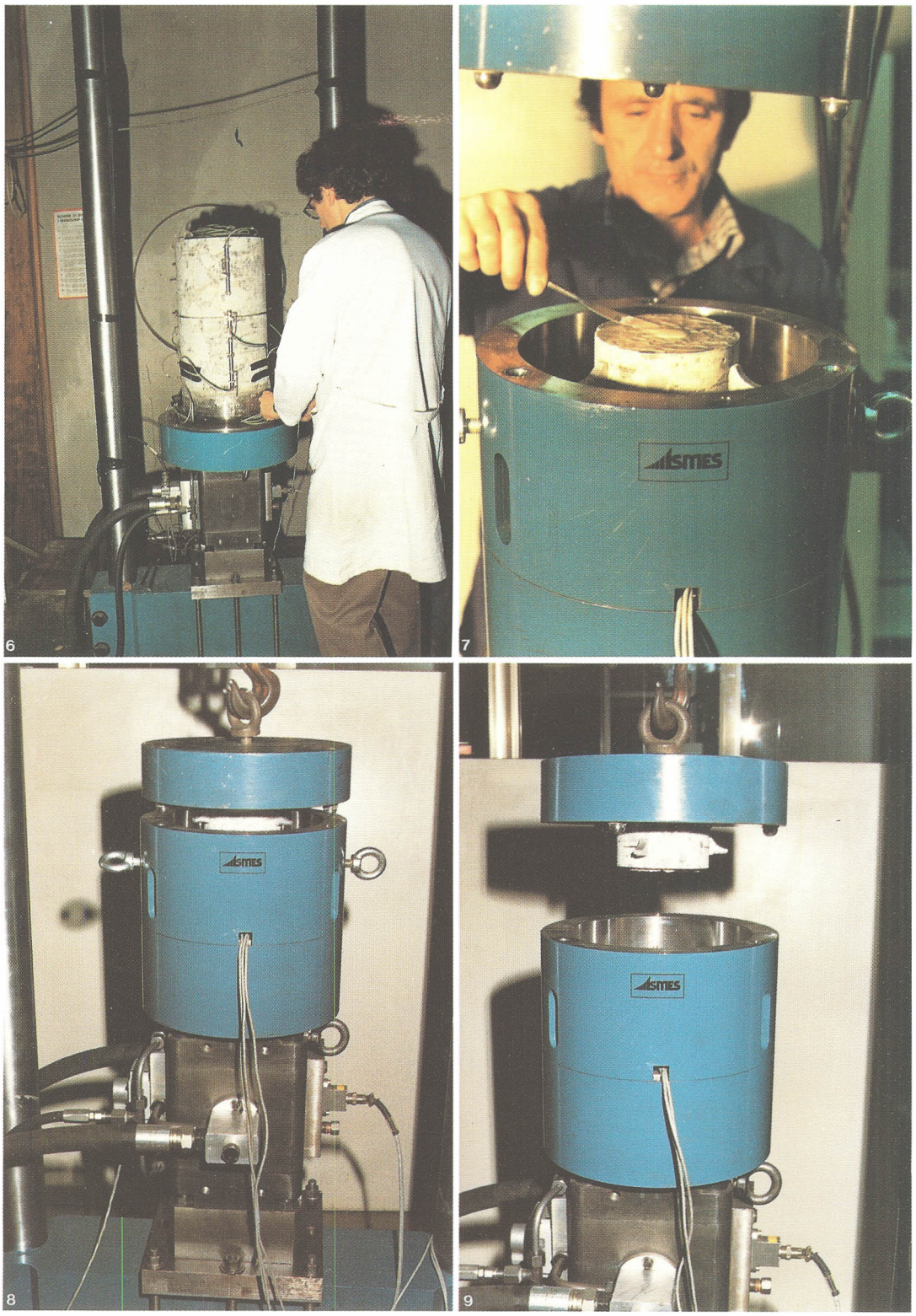

Fig. 6. Measurement of strains in upper and lower positions of specimen.
Fig. 7. Lifting of lid and application of adhesive on upper side of specimen.
Fig. 8. Relowering of lid.
Fig. 9. Conclusion of test.

Table 1.

Diameter (cm)	Number of tests	Tensile strength σ_u (MPa)	Fracture energy $\mathcal{G}_F$ (N/m)
12	14	3.32 ± 0.53	110.56 ± 30.89
18	12	3.66 ± 0.45	139.66 ± 36.32
24	11	3.31 ± 0.44	153.90 ± 20.89
30	8	2.98 ± 0.79	149.41 ± 14.31

specimens was varied between 1 and 2 for each diameter, just as the initial notch to diameter ratio was chosen to be equal to 0.1 or 0.2. In Table 1 the variability of the results with these geometrical parameters is disregarded. More details may be obtained from the original report [17].

The average values of the nominal tensile strength are plotted in Fig. 10 against the specimen diameter b in a bilogarithmic diagram. The size effect is represented by the slope of the linear regression diagram, excluding the results of the smallest specimens. It is evident how the tensile strength decreases with increasing specimen diameter.

The fracture energy instead shows the opposite trend, i.e. it increases with specimen diameter. The average values obtained experimentally are reported in Fig. 10 on the bilogarithmic plane $\ln \mathcal{G}_F$ versus $\ln b$, excluding those of the largest specimens.

Size–scale effects on tensile strength and fracture toughness have been recurrent subjects of research, as well as relevant topics, in scientific literature for the last few years. In spite of the many explanations given of the single specific trends, no unitary explanation based on very general concepts has so far been put forward. In this paper a new theoretical interpretation will be proposed according to the actual fractal nature of the reference spaces used in classical solid mechanics. A fractal space is a mathematical domain with a non-integer dimension. This is an old concept, recently reintroduced and systematized by Mandelbrot [12], Falconer [13], and other authors, which presents a wide range of applications in modern technology. For example, the weight of several

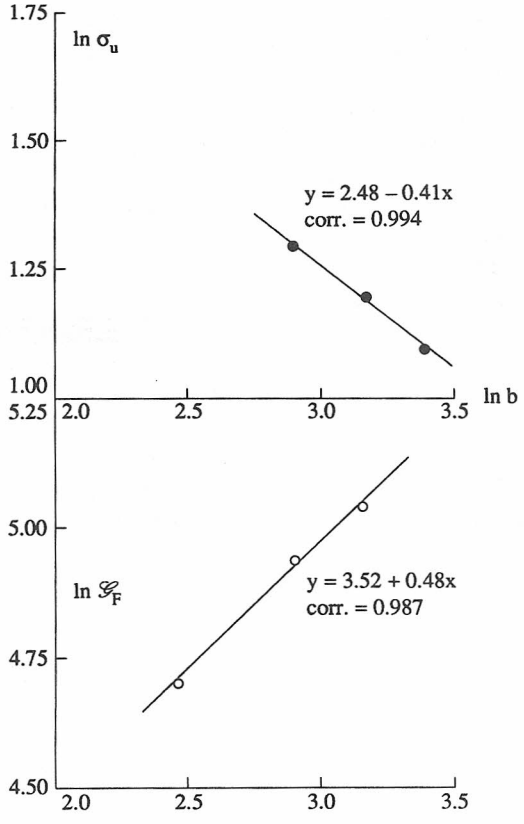

Fig. 10. Tensile strength decrease and fracture energy increase with specimen diameter.

spongy objects does not increase proportionally to the volume, because they present a non-constant classical density, understood as mass over volume, although it is possible to define a constant "universal" density, understood as mass over length raised to the fractal dimension of the space occupied by the object. This dimension is comprised between 2 and 3.

The *middle-third Cantor set*, which is a typical fractal set, may be constructed from a unit interval by a sequence of deletion operations (Fig. 11). Let E_0 be the interval [0, 1]. Let E_1 be the set obtained by deleting the middle third of E_0, so that E_1 consists of the two intervals [0, 1/3] and [2/3, 1]. Deleting the middle thirds of these intervals gives E_2; thus E_2 comprises the four intervals [0, 1/9], [2/9, 1/3], [2/3, 7/9], and [8/9, 1]. Proceeding in a like manner, E_k is obtained by deleting the middle third of each interval in E_{k-1}. Thus E_k consists of 2^k intervals, each of length 3^{-k}. The middle-third Cantor set is the intersection

$$\bigcap_{k=0}^{\infty} E_k,$$

and thus may be thought of as the limit of the sequence of sets E_k as k tends to infinity. The length of the middle-third Cantor set is zero as the limit $(2/3)^k \to 0$ for $k \to \infty$. It can be demonstrated, however, that the fractal dimension of the set is 0.631, and therefore that it can be measured consistently only as a length raised to 0.631.

A second example of a fractal set, with dimension larger than one, is the *von Koch curve* (Fig. 12). Let E_0 be a line segment of unit length. The subset E_1 consists of the four segments obtained by removing the middle third of E_0 and replacing it by the other two sides of the equilateral triangle based on the removed segment. We construct E_k by applying the same procedure to each of the segments in E_{k-1}, and so on. The sequence of polygonal curves E_k approaches the von Koch curve as k tends to infinity. The length of the von Koch curve tends to infinity as $(4/3)^k$ does for $k \to \infty$. The fractal dimension of the curve is 1.262, the dimensionality increase of 0.262 being due to its tortuosity. The curve could then be measured only as length raised to 1.262.

The systematic error that has been repeated in measuring strength and toughness of disordered materials, such as concrete and rocks, is that of considering reference areas and volumes with the ideal integer dimensions of 2 and 3, respectively. If this error is made in the scale range over which the fractal properties hold, it will be physically impossible to measure constant material properties, unless we abandon integer dimensions of the material ligament at peak stress and of the fracture surface after stress relaxation or at final rupture. Defining new tensile properties with physical dimensions depending on the fractal dimension of the damaged material microstructure represents the so-called renormalization procedure already utilized in the statistical physics of random processes [14, 15]. In this way it is possible to obtain the so-called "universal" properties, i.e. scale-invariant material constants.

Some authors have recently endeavoured to link the fractal dimension of the fracture surface to fracture toughness K_{IC} [16]. This attempt has not been successful, in particular because the physical dimension of K_{IC} was not assumed to vary with the fractal dimension of the surface. A variation in the physical dimension of fracture toughness (and hence of fracture energy), together with an analogous variation for tensile strength, turns out to provide an attenuation of the scale effects due to the dimensional disparity between strength and toughness. For a very disordered material the attenuation is complete and any scale effect vanishes, both tensile strength and fracture energy being [force] × [length]$^{-1.5}$. Similar attenuations were emphasized and analysed by the first writer for strain-hardening materials in the presence of cracks [18] and for linear elastic materials in the presence of re-entrant corners [19].

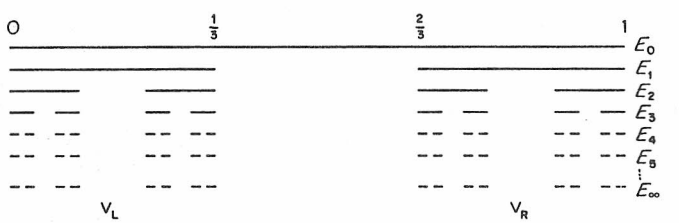

Fig. 11. Middle-third Cantor set (fractal dimension = 0.631).

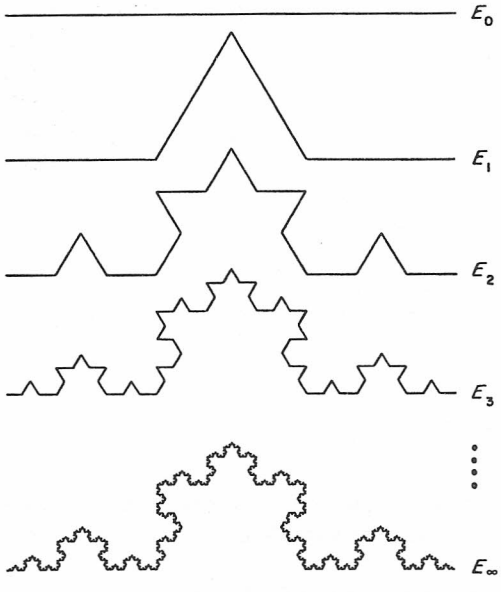

Fig. 12. von Koch curve (fractal dimension = 1.262).

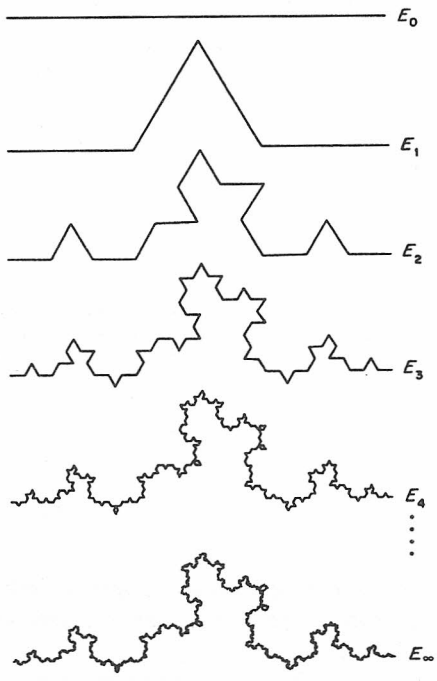

Fig. 13. Random von Koch curve.

The fractal sets that we have presented previously have random analogues. For example, in the von Koch curve construction, each time we replace the middle third of an interval by the other two sides of an equilateral triangle, we might toss a coin to determine whether to position the new part above or below the removed segment. After a few steps, we get a rather irregular-looking curve which, nevertheless, retains certain of the characteristics of the von Koch curve (Fig. 13).

The middle-third Cantor set construction may be randomized in two different ways (Fig. 14). Each time we divide a segment into three parts we could, instead of always removing the middle segment, throw a dice to decide which part to remove. Alternatively, we might choose the interval lengths at each stage of the construction at random, according to a given statistical distribution.

Whilst such random fractals do not have the self-similarity of their non-random counterparts, their non-uniform appearance is often rather closer to natural phenomena, such as coastlines, topographical surfaces, or fracture surfaces. We could say that the random fractals are *statistically self-similar* in the sense that enlargements of details have the same statistical distribution as the whole set.

5. FRACTAL NATURE OF MATERIAL LIGAMENT AND SIZE EFFECTS ON NOMINAL TENSILE STRENGTH

It is well-known that the nominal tensile strength of many materials undergoes very clear size effects. The usual trend is that of a strength decrease with size, and this is more evident for disordered (i.e. macroscopically heterogeneous and/or damaged) materials. Griffith [20] explained the strength size effect in the case of glass filaments, assuming the existence of inherent microcracks of a size proportional to the filament cross-sectional diameter. Some years later Weibull [21] gave a purely statistical explanation of the same phenomenon according to the weakest-link-in-a-chain concept. Only recently have the two views been harmonized, enriching the empirical approach of Weibull with the phenomenological assumption of Griffith [22–25]. A *statistical size distribution of self-similarity* may be defined [24, 25] for which the most dangerous defect proves to be a size proportional to the structural size. This corresponds to materials presenting a considerable dispersion in the statistical microcrack size distribution (disordered materials). In this case, the power of the LEFM stress singularity, 1/2, turns out to be the slope of the strength versus size

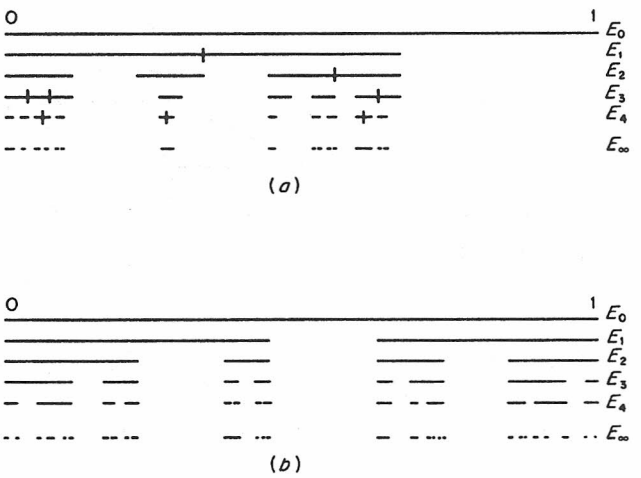

Fig. 14. Random Cantor set.

decrease in a bilogarithmic diagram. When the statistical dispersion is relatively low (ordered materials) the slope is less than 1/2 and tends to zero for regular distributions (perfectly ordered materials).

Although the above-described view contains the fractal concept of self-similarity, this is circumscribed only to the defect of maximum size, whereas the disordered nature of the material microstructure is completely disregarded. The real nature of the material will be described herein using a more complex fractal model, where the property of self-similarity is extended to the whole defect population. This model represents a more realistic picture of reality and is consistent with the fractal explanation of the fracture energy size effect, which will be proposed in the next section. On the other hand, as will be shown, slope values higher than 1/2 would represent, with both models, a degree of disorder that is so high as to be usually absent in real materials.

Let us assume that the reacting section, or ligament, of a disordered material at peak stress could be represented as a fractal space of dimension $\alpha = 2 - d_\sigma$, with $1 < \alpha \leqslant 2$ and therefore $0 \leqslant d_\sigma < 1$. The dimensionality decrement d_σ may be due to the presence of cracks and voids and hence, generally, to a cross-sectional weakening. Let us consider two bodies, geometrically similar and made up of the same disordered material (Fig. 15). If the ratio of geometrical similitude is equal to b and the *renormalized tensile strength* σ_u^* is assumed to be a material constant and to have the physical dimensions [force] × [length]$^{-(2-d_\sigma)}$, we have

$$\sigma_u^* = \frac{F_1}{1^{2-d_\sigma}} = \frac{F_2}{b^{2-d_\sigma}}, \tag{1}$$

where F_1 and F_2 are the ultimate tensile forces acting on the two bodies, respectively.

On the other hand, the apparent nominal tensile strengths are respectively

$$\sigma_u^{(1)} = \frac{F_1}{1^2} \tag{2a}$$

$$\sigma_u^{(2)} = \frac{F_2}{b^2}, \tag{2b}$$

where the latter, according to eq. (1), becomes

$$\sigma_u^{(2)} = \sigma_u^{(1)} b^{-d_\sigma}. \tag{3}$$

We can write the relationship between nominal strengths related to different sizes in logarithmic form

$$\ln \sigma_u = \ln \sigma_u(1) - d_\sigma \ln b. \tag{4}$$

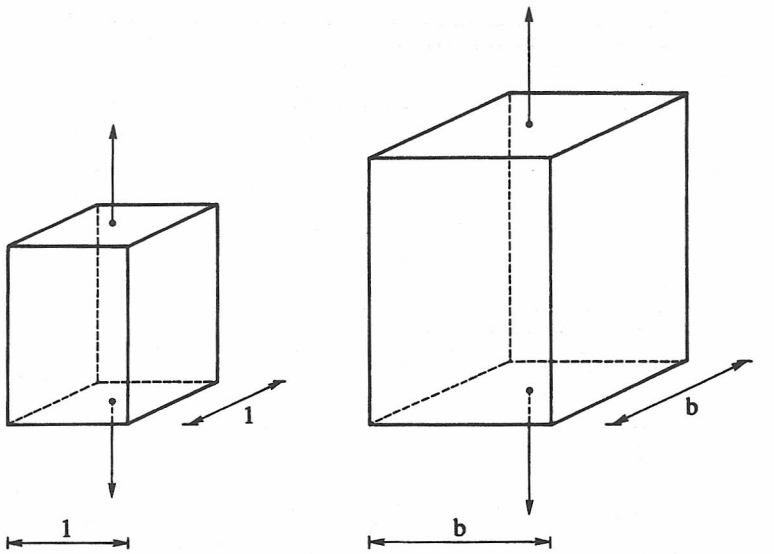

Fig. 15. Geometrically similar bodies, where b is the ratio of geometrical similitude.

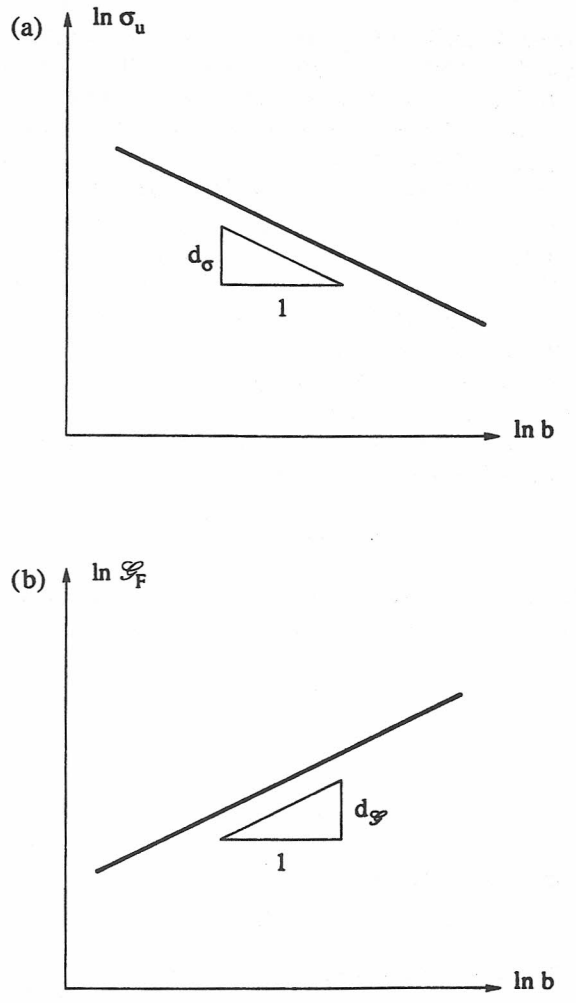

Fig. 16. (a) Nominal tensile strength decrease with specimen size. (b) Fictitious fracture energy increase with specimen size.

Equation (4) represents a straight line with slope $-d_\sigma$ in the $\ln \sigma_u$ versus $\ln b$ plane (Fig. 16(a)).

Confirmation of eq. (4) has been provided by several previous investigations, performed using different metallic or cementitious materials and with different specimen geometries: tension, bending, Brazilian, etc. These results were summarized by Carpinteri in refs [24, 25]. The same trends have been found also in the present experimental programme aimed at evaluating the true tensile properties of concrete. As may be seen from Fig. 10, the slope of the strength decrease proves to be equal to 0.41, thus revealing a material ligament of dimension 1.59. The fractal nature of the material ligament emerges very clearly at the size scales of the specimens. On the other hand, the property of self-similarity is very likely to vanish or change at higher or lower scales, owing to the limited character of the granulometric curve.

6. FRACTAL NATURE OF FRACTURE SURFACE AND SIZE EFFECTS ON FICTITIOUS FRACTURE ENERGY

It is well-known that the fracture surfaces of metals [26] and concrete [27] have a fractal nature with a roughness producing a dimensional increment with respect to the number 2. Even in this case we can detect an evident mechanical consequence, considering the size effects on fracture energy $\mathcal{G}_F$. Since Hillerborg's proposal for a concrete fracture test was published as a RILEM Recommendation [28], several researchers have measured a fracture energy $\mathcal{G}_F$ which increases with the specimen size and, more specifically, with the size of the uncracked ligament. Such a trend has been systematically found, and in each case the authors of the papers describing these experiments have tried to provide various empirical or phenomenological explanations, without, however, endeavouring to interpret their findings in a broader conceptual framework. On the other hand, if we wish to understand the experimental observations, it is necessary to abandon the classical thermodynamic concept of surface energy of an ideal solid, and to assume the energy dissipation to be occurring in a fractal space of dimension $\alpha = 2 + d_\mathcal{G}$, with $2 \leqslant \alpha < 3$ and, therefore, $0 \leqslant d_\mathcal{G} < 1$. This represents an attenuation of fracture localization due to material heterogeneity and multiple cracking.

Let us consider two bodies, geometrically similar and made up of the same disordered material (Fig. 15). If the ratio of geometrical similitude is equal to b and the *renormalized fracture energy* $\mathcal{G}_F^*$ is assumed to be a material constant and to have the physical dimensions [force] $\times$ [length]$^{-(1+d_\mathcal{G})}$, we obtain

$$\mathcal{G}_F^* = \frac{E_1}{1^{2+d_\mathcal{G}}} = \frac{E_2}{b^{2+d_\mathcal{G}}}, \tag{5}$$

where E_1 and E_2 are the energies dissipated in the two bodies, respectively.

On the other hand, the apparent fictitious fracture energies are, respectively

$$\mathcal{G}_F^{(1)} = \frac{E_1}{1^2} \tag{6a}$$

$$\mathcal{G}_F^{(2)} = \frac{E_2}{b^2}, \tag{6b}$$

where the latter, according to eq. (5), becomes

$$\mathcal{G}_F^{(2)} = \mathcal{G}_F^{(1)} b^{d_\mathcal{G}}. \tag{7}$$

We can write the relationship between fracture energies related to different sizes in logarithmic form

$$\ln \mathcal{G}_F = \ln \mathcal{G}_F(1) + d_\mathcal{G} \ln b. \tag{8}$$

Equation (8) represents a straight line with slope $d_\mathcal{G}$ in the $\ln \mathcal{G}_F$ versus $\ln b$ plane (Fig. 16(b)).

The same trends have been found in the present experimental investigation. Tensile testing performed at ISMES—Bergamo has provided a plot slope equal to 0.48 (Fig. 10), which allows a constant (universal) energy parameter to be obtained in the case where the dissipation is considered as occurring in a damaged space of dimension 2.48. It is interesting to note that the

range of self-similarity does not extend to the largest size for $\mathcal{G}_F$, just as it does not extend to the smallest size for σ_u. So the ranges of self-similarity for fracture energy and tensile strength do not necessarily coincide.

7. CONCLUSIONS

The abundant literature regarding tensile strength and fracture energy size effects as well as the newly introduced fractal theories would appear to indicate the need for a dramatic change in our conceptual framework and even in our whole way of thinking, if we want to consider and measure material constants in strength of materials as well as in fracture mechanics. This means that we have to give up ideal reference areas when we consider the tensile strength and fracture energy of disordered materials with a fractal microstructure. The so-called homogeneous materials (on the macroscopic scale or macrolevel) present, on the other hand, a very small deviation from the ideal case. Only at the microscopic scale or microlevel might they present a higher degree of fractality [29]. For concrete and rocks, for which the microlevel and the mesolevel coincide with the structural level, the tensile strength is given by a force acting on a surface having a fractal dimension lower than two, just as the fracture energy is represented by a dissipation over a surface with a fractal dimension higher than two.

In the case of tensile strength, the dimensional decrement represents self-similar weakening of the reacting cross-section or ligament, due to pores, voids, defects, cracks, aggregates, inclusions, etc. Likewise, in the case of fracture energy, the dimensional increment represents self-similar tortuosity of the fracture surface, due to aggregates and inclusions, as well as self-similar microcrack overlapping and distribution also in the direction orthogonal to that of the forming macrocrack [9].

As regards the dimensional decrement d_σ and the dimensional increment $d_{\mathcal{G}}$, experimentally they appear to be always comprised in the interval [0, 1/2]. The dimensional decrement d_σ tends to the LEFM limit 1/2 only for extremely brittle and disordered materials (defect size distribution of self-similarity) and is connected to the Weibull parameter m in the case of planar similitude [24, 25]

$$d_\sigma = \frac{2}{m}. \tag{9}$$

Even the dimensional increment $d_{\mathcal{G}}$ tends to the same limit 1/2 for extremely brittle and disordered materials. The explanation for the latter bound could arise for dimensional analysis reasons. A generalization of the *brittleness number*, as defined by the first writer [30–35], could in fact be the following:

$$s_E^* = \frac{\mathcal{G}_F^*}{\sigma_u^* b^{(1-d_\sigma-d_{\mathcal{G}})}}. \tag{10}$$

If we postulate that the reversal of the physical roles of toughness and strength is absurd, the exponent of the characteristic linear size b must be positive

$$d_\sigma + d_{\mathcal{G}} < 1. \tag{11}$$

The sum of the dimensional decrement (for material ligament) and the dimensional increment (for fracture surface) must therefore be lower than unity. On the other hand, when for very disordered materials we have $d_\sigma \simeq 1/2$, the upper bound of eq. (11) becomes $d_{\mathcal{G}} \lesssim 1/2$.

The above fractal interpretations could be regarded by some as purely mathematical abstractions, if not indeed distortions of reality. The truth is that both classical geometrical domains and fractal geometrical loci are idealizations of reality. The question that should be answered is the following: which model is closer to a real fracture trajectory in a concrete specimen, a straight line or the von Koch curve? Of course the latter, even though the fractal nature of the fracture trajectory is random and valid only in a limited scale range. This means that, for size scales tending to infinity, or, in other words, for very large specimens, tensile strength σ_u and fracture energy $\mathcal{G}_F$ may appear constant by varying the specimen size, whereas, for size scales where random

self-similarity holds, the so-called "universal properties" of the system $(\sigma_u^*, \mathcal{G}_F^*)$ are constant, although they are represented by physical quantities with unusual dimensions. The last result represents the target of the so-called "renormalization" procedure [14, 15], i.e. the determination of physical quantities that are invariant under a change of length scale.

Acknowledgements—The present research was carried out with the financial support of the Ministry for the University and for Scientific and Technological Research (MURST) and the National Research Council (CNR).

REFERENCES

[1] R. L'Hermite, Idées Actuelles sur la Technologie du Béton. *Collection de l'Institut Technique du Bâtiment et des Travaux Publics*. Paris (1955).
[2] H. Rusch and H. K. Hilsdorf, Deformation characteristics of concrete under axial tension. *Voruntersuchungen* **44** (1963).
[3] B. P. Hughes and G. P. Chapman, The complete stress-strain curves for concrete in direct tension. *Bulletin RILEM* **30,** 95–97 (1966).
[4] R. H. Evans and M. S. Marathe, Microcracking and stress-strain curves for concrete in tension. *Mater. Structures* **1,** 61–64 (1968).
[5] H. G. Heilmann, H. K. Hilsdorf and K. Finsterwalder, Festigkeit und Verformung von Beton unter Zugspannungen. *Deutscher Ausshuss für Stahl-beton* **203** (1969).
[6] P. E. Petersson, Crack growth and development of fracture zones in plain concrete and similar materials. Report TVBM-1006, Division of Building Materials, Lund Institute of Technology (1981).
[7] V. S. Gopalaratnam and S. P. Shah, Softening response of plain concrete in direct tension. *J. ACI* **82,** 310–323 (1985).
[8] H. W. Reinhardt, A. W. Cornelissen and D. A. Hordijk, Tensile tests and failure analysis of concrete. *J. Struct. Engng* **112,** 2462–2477 (1986).
[9] J. G. M. van Mier, Scaling in tensile and compressive fracture of concrete, in *Applications of Fracture Mechanics to Reinforced Concrete* (Edited by A. Carpinteri), pp. 19–31. Chapman and Hall, London (1992).
[10] D. V. Phillips and B. Zhang, Fracture energy and brittleness of plain concrete specimens under direct tension, in *Fracture Behaviour and Design of Materials and Structures* (Edited by D. Firrao), pp. 646–652. EMAS, Warley (1991).
[11] G. Ferrara and L. Imperato, Il parametro $\mathcal{G}_F$ nella meccanica della frattura del calcestruzzo: influenza della geometria di prova e del tipo di aggregato. 11*th Meeting of the Italian Section of the Society for Experimental Mechanics* (pp. 189–200), Torino, Italy (1983).
[12] B. B. Mandelbrot, *The Fractal Geometry of Nature*. W. H. Freeman and Company, New York (1982).
[13] K. Falconer, *Fractal Geometry: Mathematical Foundations and Applications*. John Wiley & Sons, Chichester (1990).
[14] K. G. Wilson, Renormalization group and critical phenomena. *Phys. Rev.* **B4,** 3174–3205 (1971).
[15] H. J. Herrmann and S. Roux (Eds), *Statistical Models for the Fracture of Disordered Media*. North-Holland, Amsterdam (1990).
[16] T. J. Mackin, J. J. Mecholsky Jr, D. E. Passoja and Y. L. Tsai, Scaling concepts applied to brittle fracture. *Proc. Symp. W*, 1990 *Fall Meeting of the Materials Research Society* (pp. 33–36), Boston, MA (1990).
[17] Programma di ricerca sperimentale sulla meccanica della frattura del calcestruzzo. Seconda parte: prove stabili a trazione, ISMES Internal Report, Doc. RAT-DPS-0586.89 (1989).
[18] A. Carpinteri, Plastic flow collapse vs separation collapse (fracture) in elastic–plastic strain-hardening structures. *Mater. Structures* **16,** 85–96 (1983).
[19] A. Carpinteri, Stress-singularity and generalized fracture toughness at the vertex of re-entrant corners. *Engng Fracture Mech.* **26,** 143–155 (1987).
[20] A. A. Griffith, The phenomenon of rupture and flow in solids. *Phil. Trans. R. Soc. Lond.* **A221,** 163–198 (1921).
[21] W. Weibull, *A Statistical Theory of the Strength of Materials*. Swedish Royal Institute for Engineering Research, Stockholm (1939).
[22] A. M. Freudenthal, Statistical approach to brittle fracture, in *Fracture* (Edited by H. Liebowitz), Vol. 2, pp. 591–619. Academic Press, New York (1968).
[23] A. S. Jayatilaka, *Fracture of Engineering Brittle Materials*. Applied Science, London (1979).
[24] A. Carpinteri, *Mechanical Damage and Crack Growth in Concrete: Plastic Collapse to Brittle Fracture*. Martinus Nijhoff Dordrecht (1986).
[25] A. Carpinteri, Decrease of apparent tensile and bending strength with specimen size: two different explanations based on fracture mechanics, *Int. J. Solids Structures* **25,** 407–429 (1989).
[26] B. B. Mandelbrot, D. E. Passoja and A. J. Paullay, Fractal character of fracture surfaces of metals. *Nature, Lond.* **308,** 721–722 (1984).
[27] V. E. Saouma, C. C. Barton and N. A. Gamaleldin, Fractal characterization of fracture surfaces in concrete. *Engng Fracture Mech.* **35,** 47–53 (1990).
[28] RILEM Technical Committee 50, Determination of the fracture energy of mortar and concrete by means of three-point bend tests on notched beams, Draft Recommendation. *Mater. Structures* **18,** 287–290 (1985).
[29] P. Meakin, Models for material failure and deformation. *Science* **252,** 226–234 (1991).
[30] A. Carpinteri, Experimental determination of fracture toughness parameters K_{IC} and J_{IC} for aggregative materials. *Proc. 5th Int. Conf. Fracture* (pp. 1491–1498). Pergamon Press, Oxford (1981).
[31] A. Carpinteri, Static and energetic fracture parameters for rocks and concretes. *Mater. Structures* **14,** 151–162 (1981).
[32] A. Carpinteri, Notch sensitivity in fracture testing of aggregative materials. *Engng Fracture Mech.* **16,** 467–481 (1982).
[33] A. Carpinteri, Interpretation of the Griffith instability as a bifurcation of the global equilibrium, in *Applications of Fracture Mechanics to Cementitious Composites* (Edited by S. P. Shah), pp. 287–316. Martinus Nijhoff, Dordrecht (1985).

[34] A. Carpinteri, Limit analysis for elastic-softening structures: scale and slenderness influence on the global brittleness, in *Brittle Matrix Composites* (Edited by A. M. Brandt and I. H. Marshall), pp. 497–508. Elsevier Applied Science, London and New York (1986).
[35] A. Carpinteri, Cusp catastrophe interpretation of fracture instability. *J. Mech. Phys. Solids* **37,** 567–582 (1989).

(*Received* 14 *June* 1993)